Harmonically trapped imbalanced quantum droplets

T. A. Flynn ⬤,* N. A. Keepfer ⬤, N. G. Parker ⬤, and T. P. Billam ⬤

Joint Quantum Centre (JQC) Durham-Newcastle, School of Mathematics, Statistics and Physics, Newcastle University,
Newcastle upon Tyne, NE1 7RU, United Kingdom

A two-component quantum droplet is an attractive mixture of ultracold bosons stabilized against collapse by quantum fluctuations. Commonly, two-component quantum droplets are studied within a balanced mixture. However, the mixture can be imbalanced resulting in a lower energy but less stably bound droplet, or even a droplet submerged in a gas. This work focuses on the experimentally relevant question: how are imbalanced droplets modified by harmonic trap potentials? Droplet ground states and breathing modes are analyzed across the two-dimensional parameter space of imbalance and trap strength. The robustness of the droplet imbalance is also studied by releasing the droplet from the trap, demonstrating that this can lead to the creation of free-space, imbalanced droplets.

I. INTRODUCTION

Quantum gases have developed into a rich platform to study a variety of physics from analogs of condensed matter and many-body systems, [1–3], to simulators of cosmological processes [4–6]. Much of the theoretical and experimental results of these studies are dominated by mean-field (MF) contributions. At ultracold temperatures quantum mechanical effects are pronounced, enabling the study of beyond-mean-field (BMF) contributions, i.e., quantum fluctuations. Two-component quantum droplets are one such quantum gas system in which quantum fluctuations are significant [7,8].

The quantum droplets considered here are formed of three-dimensional (3D) ultracold mixtures of atomic Bose gases in which the interactions between the two species are tuned to be dominantly attractive. Two-body interactions, characterized by the scattering length, a_s, can be controllably tuned via a Feshbach resonance [9–11]. Taking into account only MF physics, these attractive mixtures would be unstable to collapse. The contraction of the cloud leads to an increased density and consequently an increased contribution from the BMF corrections. Quantum fluctuations, described to first order by the Lee-Huang-Yang (LHY) correction [12], lead to an effective repulsion between the atoms that balances the attraction forming a self-bound, dilute liquid droplet [7,8]. Therefore, quantum droplets are an experimentally observable state of matter in which quantum fluctuations not only contribute, but are integral. It should be noted that the BMF stabilized collapse does not carry across to the single-component Bose gas, which has been experimentally demonstrated to be unstable under attractive two-body interactions [13,14].

Though quantum droplets were first predicted in 3D mixtures of Bose gases, it has been shown that quantum droplets can be formed in other quantum gas systems [15,16]. Aside from three dimensions, quantum droplets can also be formed in low-dimensional mixtures [17]; however, the form of the LHY correction varies with dimensionality [17–19]. For example, in one dimension the mechanism for droplet formation is the reverse of three dimensions, i.e., the two-body interactions are dominantly repulsive and stabilize attraction from quantum fluctuations [17]. The intermediate case of two dimensions can have both repulsive and attractive contributions from the LHY correction [17]. Beyond mixtures, quantum droplets have also been widely studied in dipolar quantum gases [20–23], where quantum fluctuations stabilize a collapse from long-ranged, anisotropic attractive interactions [24] resulting in anisotropic droplet profiles [25–29].

As indicated above, quantum gases are a platform for probing physics from areas that appear disparate. One field that has benefited from a close connection with quantum gases is fluid dynamics. Many quantum gases exhibit superfluidity, which has been used as an analog to the dynamics of classical fluids such as vortex dynamics [30] or turbulence [31,32]. Quantum droplets are a further extension of this tradition as they can be used to probe liquid properties such as surface tension [7,33,34] and incompressibility [35,36].

Two-component quantum droplets have been experimentally observed in both homonuclear ^{39}K [36–39] and heteronuclear, ^{41}K-^{87}Rb and ^{23}Na-^{87}Rb [40,41], mixtures. The benefit of using homonuclear mixtures is the precise control over the population numbers of each component. Homonuclear mixtures are made of atoms prepared in different hyperfine states. Experiments begin with all atoms in one component; a radio frequency pulse is then used to controllably transition a proportion of the atoms to the second component. This control allows for probing one of the predictions of two-component droplets: density balancing.

---

*t.flynn@ncl.ac.uk

The original droplet prediction of Ref. [7] argues that a density balance is preserved during the droplet formation. This density balance is due to an energetic favorability for the two-component densities to maintain a fixed ratio $n_2/n_1 =$ const. where n_i is the number density of the ith component. The majority of theoretical studies of two-component quantum droplets assume density balancing. Removing the assumption of density balancing gives the freedom to explore droplets with imbalanced component population numbers. Imbalanced droplets have been studied in one dimension [42], confined to both a ring [43] and an optical lattice [44]. There have also been works exploring 3D imbalanced droplets in free space [45] and confined to a toroidal trap [46]. Imbalanced droplets have also been theoretically studied in the growing area of dipolar mixtures [47,48].

Imbalanced droplets fall into two main regimes [7,45]: (i) bound, imbalanced droplets, in which there is a population imbalance in the droplet core; (ii) saturated, imbalanced droplets, corresponding to a droplet core that is saturated with majority-component atoms, with any further majority component surrounding the droplet as an unbound gas.

Reference [45] studied the ground states and breathing modes of imbalanced quantum droplets in free space, and showed that a droplet can lower its total energy by absorbing atoms into one of its components. The decrease in total energy corresponds to an increase in the energy per particle, indicating that imbalanced droplets are less stably bound, which is demonstrated further by the larger parameter space of unstable breathing modes of such droplets due to particle shedding. The primary focus of this paper is to investigate how the ground states and breathing modes are modified with the application of an isotropic harmonic trap. These investigations are motivated by the experimental feasibility of creating and probing harmonically trapped imbalanced quantum droplets. Additionally, this work explores the stability of these droplets when released into free space across a variety of timescales.

This work starts by defining the theory used to model quantum droplets in Sec. II. This model is first implemented in Sec. III to explore how the imbalanced droplet ground states are modified by isotropic, harmonic trapping potentials. Section IV looks at propagating these ground states in time, subject to an initial perturbation, to analyze the droplet breathing modes, both for varying trap strength, and size of imbalance. Section V investigates the stability of imbalanced droplets under an instantaneous and linearly ramped removal of the trapping potential, as these are methods widely used in quantum gas experiments. Finally, the main conclusions and future work are discussed in Sec. VI.

II. MODEL

A zero-temperature mixture of two weakly interacting, dilute, homonuclear Bose gases can be described by the energy functional [7,49]

$$
E = \int \left[\frac{\hbar^2}{2m} |\nabla \Psi_1|^2 + \frac{\hbar^2}{2m} |\nabla \Psi_2|^2 + V_1 |\Psi_1|^2 \right.
$$
$$
\left. + V_2 |\Psi_2|^2 + \mathcal{E}_{\mathrm{MF}} + \mathcal{E}_{\mathrm{LHY}} \right] d^3 \mathbf{r}, \tag{1}
$$

in which m is the atomic mass of both components and V_i is the trapping potential applied to the ith component. The first two terms of Eq. (1) are the kinetic energy contributions, while $\mathcal{E}_{\mathrm{MF}}$ is the MF energy density term given by,

$$
\mathcal{E}_{\mathrm{MF}} = \frac{2\pi \hbar^2 a_{11}}{m} |\Psi_1|^4 + \frac{2\pi \hbar^2 a_{22}}{m} |\Psi_2|^4 + \frac{4\pi \hbar^2 a_{12}}{m} |\Psi_1|^2 |\Psi_2|^2,
$$

where a_{ii} and a_{12} are the intra- and interspecies scattering lengths. The final term, $\mathcal{E}_{\mathrm{LHY}}$, is the energy density of the LHY correction, which, to first order, describes the effects of quantum fluctuations on the condensate [12]. For a homonuclear bosonic mixture the LHY correction takes the analytic form [7]

$$
\mathcal{E}_{\mathrm{LHY}} = \frac{256\sqrt{\pi}\hbar^2}{15m} \left(a_{11} |\Psi_1|^2 + a_{22} |\Psi_2|^2 \right)^{5/2}. \tag{2}
$$

The LHY energy density does not depend on a_{12} due to the assumption that the mixtures lies at the critical point of attractive instability, i.e., $a_{12}^2 = a_{11}a_{22}$, removing the issue of complex contributions resulting from an unstable phonon mode [7,50,51]. It should be noted that this approximation is made only in the derivation of Eq. (2), and does not imply any parameter choice in later sections.

The energy functional in Eq. (1) can be minimized via the variational relation $i\hbar(\partial \Psi_i/\partial t) = \delta E/\delta \Psi_i^*$, giving the equal-mass, coupled extended GP equations [7]

$$
i\hbar \frac{\partial \Psi_1}{\partial t} = \left[-\frac{\hbar^2}{2m}\nabla^2 + V_1 + \frac{4\pi\hbar^2}{m}\left(a_{11}|\Psi_1|^2 + a_{12}|\Psi_2|^2\right) \right.
$$
$$
\left. + \frac{128\sqrt{\pi}\hbar^2 a_{11}}{3m}\left(a_{11}|\Psi_1|^2 + a_{22}|\Psi_2|^2\right)^{3/2} \right]\Psi_1,
$$
$$
i\hbar \frac{\partial \Psi_2}{\partial t} = \left[-\frac{\hbar^2}{2m}\nabla^2 + V_2 + \frac{4\pi\hbar^2}{m}\left(a_{22}|\Psi_2|^2 + a_{12}|\Psi_1|^2\right) \right.
$$
$$
\left. + \frac{128\sqrt{\pi}\hbar^2 a_{22}}{3m}\left(a_{11}|\Psi_1|^2 + a_{22}|\Psi_2|^2\right)^{3/2} \right]\Psi_2. \tag{3}
$$

The dimensional scalings $\mathbf{r} = \xi \tilde{\mathbf{r}}$, $t = \tau \tilde{t}$ and $\Psi_i = \rho_i^{1/2} \tilde{\Psi}_i$ result in the dimensionless, equal-mass coupled extended GP equations,

$$
i\frac{\partial \Psi_1}{\partial t} = \left[-\frac{1}{2}\nabla^2 + V_1 + |\Psi_1|^2 + \eta|\Psi_2|^2 \right.
$$
$$
\left. + \alpha\left(|\Psi_1|^2 + \beta|\Psi_2|^2\right)^{3/2} \right]\Psi_1,
$$
$$
i\frac{\partial \Psi_2}{\partial t} = \left[-\frac{1}{2}\nabla^2 + V_2 + \beta|\Psi_2|^2 + \eta\beta|\Psi_1|^2 \right.
$$
$$
\left. + \alpha\beta^2\left(|\Psi_1|^2 + \beta|\Psi_2|^2\right)^{3/2} \right]\Psi_2, \tag{4}
$$

in which all tildes have been neglected and the dimensionless parameters are

$$
\eta = \frac{a_{12}}{\sqrt{a_{11}a_{22}}}, \quad \beta = \left(\frac{a_{22}}{a_{11}}\right)^{1/2},
$$
$$
\alpha = \frac{32}{3}\left[\frac{2}{3\pi} \frac{|\delta a| a_{11}^{5/2} n_1^{(0)}}{\sqrt{a_{11}} + \sqrt{a_{22}}} \right]^{1/2},
$$

with dimensional parameters

$$\xi = \sqrt{\frac{3}{8\pi} \frac{\left(\sqrt{a_{11}} + \sqrt{a_{22}}\right)}{|\delta a|\sqrt{a_{11}} n_1^{(0)}}}, \quad \tau = \frac{3m}{8\pi\hbar} \frac{\left(\sqrt{a_{11}} + \sqrt{a_{22}}\right)}{|\delta a|\sqrt{a_{11}} n_1^{(0)}},$$

$$\rho_1 = \frac{2}{3} \frac{|\delta a| n_1^{(0)}}{\sqrt{a_{11}}\left(\sqrt{a_{11}} + \sqrt{a_{22}}\right)}, \quad \rho_2 = \frac{2}{3} \frac{|\delta a| n_1^{(0)}}{\sqrt{a_{22}}\left(\sqrt{a_{11}} + \sqrt{a_{22}}\right)},$$

where $\delta a = a_{12} + \sqrt{a_{11}a_{22}}$ and $n_1^{(0)}$ is the equilibrium density of component 1 for the balanced mixture [7]. The expression of the equilibrium density is calculated in a homogeneous infinite system under the criterion of a vanishing pressure, i.e., the droplet in equilibrium with the vacuum, and takes the form [7]

$$n_1^{(0)} = \frac{25\pi}{1024} \frac{\left(a_{12} + \sqrt{a_{11}a_{22}}\right)^2}{a_{11}^{3/2} a_{22} \left(\sqrt{a_{11}} + \sqrt{a_{22}}\right)^5}.$$

The density scalings ρ_i correspond to rescaled normalization constants, $\tilde{N}_i = N_i/(\rho_i \xi^3)$, in which N_i is the population of the ith-component wave function. By breaking the assumption of density locking, it is possible to imbalance the population numbers such that $N_2/N_1 \neq \sqrt{a_{11}/a_{22}}$.

The trapping potentials are nondimensionalized by $V_i = \left(m\xi^2/\tau^2\right)\tilde{V}_i$. This work only considers isotropic harmonic trapping with equal traps applied to each component, i.e., $V_i = V = \frac{1}{2}m\omega_r^2 r^2$. Under nondimensionalization this becomes $\tilde{V} = \frac{1}{2}\tilde{\omega}_r^2 \tilde{r}^2$, in which $\tilde{\omega}_r^2 = \left(\tau\xi^2 m/\hbar\right)\omega_r^2$. In subsequent sections the dimensionless population numbers and trapping potentials are presented without tildes, as only dimensionless parameters are used hereafter.

The results in this paper will be contrasted with the density-locked model, used widely in modeling quantum droplet experiments [36,37,39]. The density-locked model assumes a constant density ratio, $n_2/n_1 = \sqrt{a_{11}/a_{22}}$, such that the two-component wave functions can be expressed in terms of a single wave function, $\Psi_i = \sqrt{n_i}\phi$, neglecting any out-of-phase motion between the components [7,52,53]. Under these assumptions, Eqs. (3) can be nondimensionalized and reduced to a single equation,

$$i\frac{\partial\phi}{\partial t} = \left[-\frac{1}{2}\nabla^2 - 3|\phi|^2 + \frac{5}{2}|\phi|^3\right]\phi,$$

with the system described by a single parameter, an effective atom number, $\tilde{N}$, given by [7]

$$\tilde{N} = \left(\frac{\sqrt{a_{22}}}{n_1^{(0)}\left(\sqrt{a_{11}} + \sqrt{a_{22}}\right)}\right)\frac{N}{\xi^3}, \tag{5}$$

in which N here is the total atom number $N = N_1 + N_2$. Within this work, balanced and imbalanced droplets are both modeled by Eqs. (4), though it should be noted that for a balanced droplet the dimensionless parameters $(N_1, N_2, \alpha, \beta, \eta)$ can be recast to $\tilde{N}$. In the density-locked model a given set of scattering lengths, a_{ii} and a_{12}, correspond to a fixed population number ratio, $N_2/N_1 = \sqrt{a_{11}/a_{22}}$.

III. GROUND STATES

How the density of a spherically symmetric balanced droplet varies with harmonic trap frequency has been studied

in Ref. [54]. The trap frequency can be considered low if there is no significant change from the free-space droplet density, whereas a higher-frequency trap eventually leads to the flat-top density of large droplets being lost. Furthermore, in free space the negative chemical potential, $-\mu$, is described as the particle emission threshold of the droplet, however, this description breaks down in a trap [54]. It can therefore be argued that in the trap-dominated regime the idea of a droplet begins to be less defined, and the mixture transitions to a trapped gas. Reference [54] approximates the transition to the trap-dominated regime as the point in which the potential energy at the droplet surface becomes comparable to the binding energy of the droplet, resulting in $\omega_r^{(c)} \sim \left(4\pi/3\tilde{N}\right)^{1/3}$ where $\tilde{N}$ is the effective atom number of the density-locked model in Eq. (5) [7].

One main assumption of this work is spherical symmetry. Density is assumed to be a function of radius only, reducing the computational problem to an effective 1D system with the kinetic term becoming $\nabla^2\Psi_i \to \left[\partial^2(r\Psi_i)/\partial r^2\right]/r$. Another assumption of this work is balanced intraspecies scattering lengths $(a_{11} = a_{22} \Rightarrow \beta = 1)$. Thus, the only possibly difference between components is from an imposed population number imbalance of $N_1 = N_2 + \delta N_1$. To find ground states, Eqs. (4) are evaluated numerically in imaginary time until the energy of the mixture is adequately converged.[1] The numerical scheme is a fourth-order Runge-Kutta method, using a second-order centred finite-difference scheme for the spatial derivatives. Neumann boundary conditions $(\partial\Psi_i/\partial r = 0)$ are applied at $r = 0$ and at $r = L_r$, where L_r is the radial computational box size. Note that for all simulations presented in this work, $\omega_r^{(c)} \approx 0.186$.

Figure 1(a) shows balanced (purple) and imbalanced (orange) droplet density profiles in a trap with frequency $\omega_r \approx 0.0442$. Figure 1(b) presents an example of the imbalanced atoms forming a significant gas density around the surface of the droplet in a trap with higher frequency $\omega_r \approx 0.353$. Figure 1(a) shows that the imbalanced and balanced droplets have comparable density profiles, whereas Fig. 1(b) shows a more considerable deviation between the balanced and imbalanced droplets, in a higher-frequency trap. The central density splitting becomes more pronounced in the higher-frequency trap, showing a more suppressed minority-component central density.

The divergence of the two chemical potentials with increasing imbalance is a key observation of Ref. [45]. For increasing trap frequency the chemical potential of a balanced droplet increases, eventually becoming positive as the density of the mixture significantly deviates from the free-space droplet density. Figure 1(c) presents chemical potential data, defined by a 2D parameter space of imbalance and trap frequency $(\delta N_1, \omega_r)$, where $\omega_r \approx \{0.00441, 0.0662, 0.128, 0.190\}$, i.e., showing trap frequencies up to approximately $\omega_r^{(c)}$.

Figure 1(c) shows that the two-component chemical potentials of balanced droplets are equal and increase with

_____

[1]To check for ground-state convergence, the energy difference between two successive time steps, ϵ_{diff}, is used. The tolerance for convergence is $\epsilon_{\text{diff}} \lesssim 10^{-8}$.
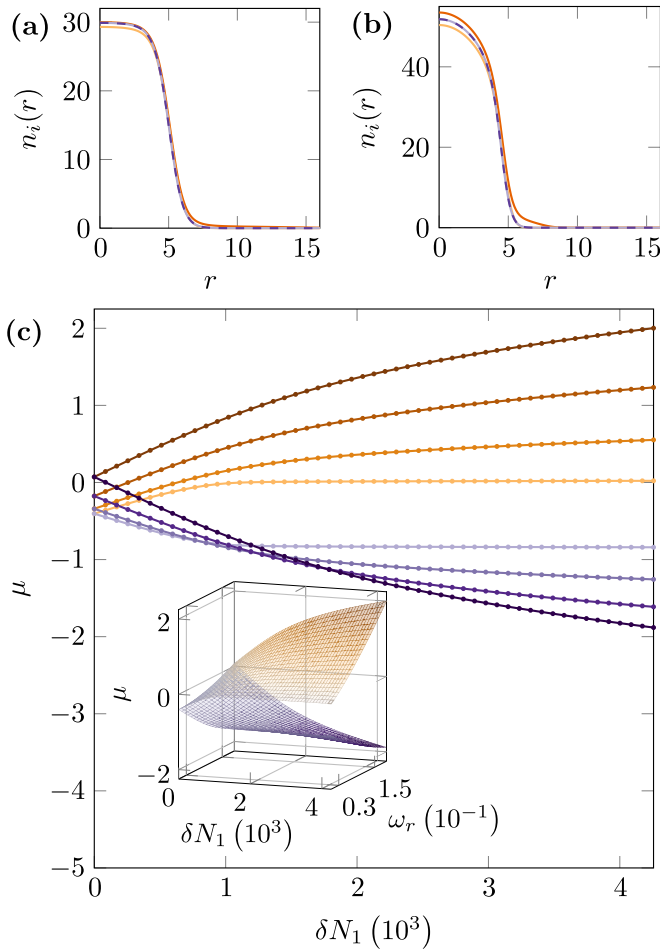
FIG. 1. Balanced and imbalanced quantum droplets in isotropic harmonic traps (with, $N_2 \approx 17027$, $\alpha \approx 0.00657$, and $\eta \approx -1.11$). (a) Droplet ground-state density profiles, of size $\bar{N} \approx 649$ with balanced components, $\delta N_1 = 0$, (the light and dark purple dashed lines) and an imbalance of $\delta N_1 \approx 8513$ (majority component, dark orange; minority component, light orange), in a trap of frequency $\omega_r \approx 0.0442$. (b) Equivalent balanced and imbalanced droplet to (a), but with a trapping frequency of $\omega_r \approx 0.353$. (c) Majority (orange) and minority (purple) chemical potentials across the 2D parameter space of imbalance and trap frequency, i.e., $(\delta N_1, \omega_r)$, for the fixed droplet size considered in (a) and (b), at trap frequencies of $\omega_r \approx \{0.00441, 0.0662, 0.128, 0.190\}$, with $0 \leqslant \delta N_1 \lesssim 4257$. The inset shows the surfaces for the majority (orange) and minority (purple) component chemical potentials across the 2D parameter space for which the curves in (c) are 1D slices of set ω_r values. Note that the two surfaces are equal at $\delta N_1 = 0$ imbalance, but diverge for increasing imbalance.

trap frequency, in agreement with Ref. [54]. Beyond the balanced case, the lowest-frequency trap ($\omega_r \approx 0.00441$) shows similar behavior to the free-space chemical potentials presented in Ref. [45], in that the chemical potentials appear to reach a saturation limit, though there will be effects from the unbound gas such that these curves are approximate to the saturated limit. For the higher trap frequencies of $\omega_r \approx \{0.0663, 0.128, 0.190\}$, the two chemical potentials diverge with the majority-component chemical potential becoming large and positive, while the minority-component chemical

potential becomes large and negative. The diverging chemical potentials represent a clear distinction between balanced and imbalanced trapped droplets, and an excerpt of the 2D parameter space is included in the inset of Fig. 1(c), with the majority and minority chemical potentials plotted as orange and purple surfaces, respectively, demonstrating the chemical potentials diverging for increased trap strength and imbalance.

Adding harmonic traps to both balanced and imbalanced droplets causes the flat-topped density profile to eventually be lost with increasing trap frequency. One key difference between balanced and imbalanced droplets is that the trap causes any unbound atoms to form a trapped gas at the droplet surface. For balanced droplets the chemical potential increases with trap frequency until eventually becoming positive. Whereas, for imbalanced droplets it is always possible for the minority-component chemical potential to be made negative in isotropic harmonic traps by tuning the imbalance. One way to understand the effect that this squeezed external gas cloud has on the droplet is to analyze the breathing modes of the droplets.

IV. BREATHING MODES

To initiate the breathing mode dynamics of trapped droplets, a perturbation is made by imprinting a harmonic potential of the form $e^{i\epsilon r^2}$, where ϵ is small (here $\epsilon = 10^{-5}$) onto the minority-component ground-state wave function [55,56]. This perturbed ground state is then propagated in real time.

The breathing modes of balanced droplets in free space have two regimes, self-evaporative and non-self-evaporative [7,57]. In the self-evaporative regime the breathing mode is unstable because the mode frequency exceeds the particle emission threshold, $-\mu$. Hence, the droplet will emit atoms to lower its energy, corresponding to a decaying sinusoidal oscillation with a frequency that asymptotes to the particle emission threshold, $-\mu$. In the non-self-evaporative regime, the breathing mode frequency does not exceed the particle emission threshold therefore the mode is stable and nondecaying. Additionally, the frequency of the balanced droplet breathing mode varies with droplet size only [7].

Breathing modes in imbalanced droplets are instead dominated by unstable regions. For both self-evaporative and non-self-evaporative droplets, an imbalance implies an unstable, decaying breathing mode except for small imbalances in the non-self-evaporative regime [45].

In this analysis, the focus will be on decaying breathing modes (i.e., excluding non-self-evaporative droplets that are either balanced or have sufficiently small imbalances). Trapped balanced droplets exhibiting nondecaying breathing modes have already been studied in Ref. [54]. To examine the breathing modes of trapped, imbalanced droplets, this section will take one example droplet size, $\bar{N} \approx 649$ (as in Fig. 1). Different droplet sizes yield qualitatively the same behavior, with only a difference in mode frequency. By fixing droplet size, the system is again reduced to a 2D parameter space in imbalance and trap frequency, $(\delta N_1, \omega_r)$. The remainder of this section is split into two subsections: first, breathing modes are observed with varying trap strengths with small imbalances, of a similar magnitude to those in Fig. 1(c); second,

trap frequency is fixed allowing for breathing modes to be observed with imbalances much larger than those in Fig. 1(c).

A. Varying trap strength

The top panel of Fig. 2(a) shows an example of a self-evaporative, balanced droplet in a trap of frequency $\omega_r \approx 0.00883$. The data shown is a measure of the droplet central density, $\bar{n}_i(t) = n_i(r = 0, t) - \langle n_i(r = 0) \rangle_t$, where $\langle \cdots \rangle_t$ represents time averaging. The droplet exhibits a decaying oscillation due to the emission of particles, causing the droplet to asymptotically relax to a lower-energy state. However, the emitted particles are refocused by the trap back toward the droplet resulting in the short-lived, high-amplitude oscillations, which are the result of a recombination event between the droplet and the reabsorbed wave packet. This then leads to the self-evaporation reoccurring at set intervals of approximately half the associated trap period of $T = 2\pi/\omega_r \approx 712 = 2 \times 356$ with $t = 356$ being the approximate time for the reinitialized decay in Fig. 2(a).

The balanced droplet recombination can be thought of as clean, as there is little noise produced and the reinitialized oscillation is approximately equivalent to the initial oscillations. In the presence of an imbalance ($\delta N_1 \approx 4257$), given in the bottom panel of Fig. 2(a), the recombination events are not clean as each separate repetition of decaying oscillation is not equivalent to the previous. The trapped, unbound atoms alter the recombination of the emitted particles. Eventually these recombination events will lead to significant noise and thus the remainder of the analysis presented here will focus on the dynamics prior to the first recombination event.

Figures 2(b), 2(c) and 2(d) show the same self-evaporative droplet given in Fig. 2(a) with an imbalance of $\delta N_1 \approx 4257$, for three trap frequencies $\omega_r \approx \{0.00662, 0.0106, 0.0309\}$, with each figure showing times before the first recombination event. The data presented is the same measure of central density as in Fig. 2(a), with insets of the associated power spectra $|\mathcal{F}'[\bar{n}_i]|^2$ in which $\mathcal{F}'[\cdot]$ denotes the power spectrum rescaled by the mean, and all negative frequencies set to zero purely for better data visualization. The time periods are chosen to highlight the behavior of the modes, largely after the decay of the initial mode, except for in Fig. 2(d), discussed further below.

The breathing mode dynamics of an imbalanced droplet in a trap of frequency $\omega_r \approx 0.00662$ are given in Fig. 2(b). These dynamics exhibit the three distinct modes of the equivalent free-space droplet (with the associated three peaks given in the inset power spectrum) [45]. The near-zero frequency peak in the power spectrum of the majority component corresponds to the free-space majority component chemical potential, and is the highest amplitude mode. The effect of this mode can be seen by the relative difference in oscillation between the two components in Fig. 2(b). There is also the superposition of two other modes, which are of comparable amplitude in both the majority and minority component, corresponding to the intrinsic droplet breathing mode (the central peak of the inset), i.e., the initial, high-amplitude mode, and the minority-component chemical potential (the highest-frequency mode in the inset).

Increasing the trap frequency to a balanced droplet corresponds to a relatively small increase in breathing mode
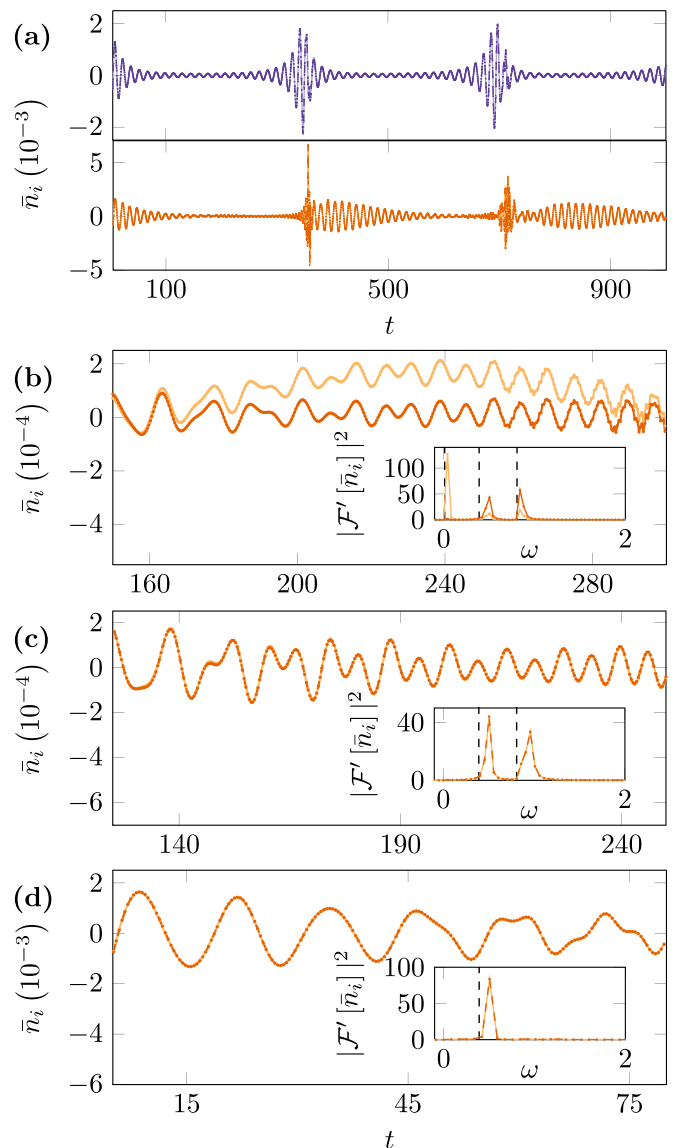

FIG. 2. Breathing modes of trapped imbalanced droplets. (a) Droplet central densities in time for both a self-evaporative, balanced (top) and imbalanced (bottom) droplet (with imbalance $\delta N_1 \approx 4257$) in a trap with frequency $\omega_r \approx 0.00883$. The droplet is defined with the same parameters as in Fig. 1. Note the recombination events that cause the self-evaporative dynamics to be reinitiated. (b) Droplet central density for the $\delta N_1 \approx 4257$ imbalanced droplet in the bottom panel of (a), in a trap with $\omega_r \approx 0.00662$. The trap frequency is sufficiently low such that all three modes, i.e., the intrinsic mode, and the two modes corresponding to the two chemical potentials, can be observed before the first recombination event. (c) A higher trap frequency of $\omega_r \approx 0.0106$ showing that the shorter period between recombination events no longer allows for the long wavelength oscillation of the majority component. (d) An increased trap frequency of $\omega_r \approx 0.0309$. The recombination events occur within such short intervals that the dynamics are dominated by the intrinsic droplet breathing mode as there is not sufficient time for this mode to decay.

frequency [54], and this effect appears to carry over to the trapped, imbalanced droplet. The inset power spectrum of Fig. 2(b) includes the three free-space breathing modes given by the vertical, dashed lines. All three of these modes have

an upshifted frequency due to the trap, though this increase is small due to the relatively low trap frequency.

Figure 2(c) shows that if the trap frequency is increased, eventually the highest-amplitude mode is lost. By increasing the trap frequency to $\omega \approx 0.0106$, the two component central densities oscillate in phase with one another, i.e., there is no long-wavelength oscillation between the two components as given in Fig. 2(b). The low-frequency mode cannot oscillate within the reduced period between recombination events from the increased trap frequency.

Figure 2(d) shows the highest trap frequency, $\omega_r \approx 0.0309$, considered in this section. At this trap frequency, the period between recombination events is considerably shortened. Hence the time window in focus is dominated by the initial, high-amplitude mode of the droplet, shown by the single peak in the inset power spectrum. There are some interactions with other modes at the later times shown in Fig. 2(d), but there is not sufficient time for the initial mode to decay.

No higher trap frequencies are studied here because the high recombination rate implies only the intrinsic mode is observable. Note too that this highest trapping frequency is still an order of magnitude smaller than $\omega_r^{(c)} \approx 0.188$.

In summary, there is a close relationship in the dynamics between imbalanced droplets in free space and in harmonic traps. For low trap frequencies the three breathing modes of the free-space, imbalanced droplet are visible. However, increasing the trap frequency leads to the loss of the majority component mode. Eventually for higher trap frequencies, the oscillations are dominated by the intrinsic droplet mode, as there is not sufficient time between recombination events for the initial mode to decay, resulting in the loss of the minority-component mode. The recombination events in higher-frequency traps lead to dynamics rapidly dominated by excitations. Therefore, if the multiple breathing modes of trapped imbalanced droplets were to be experimentally observed, it is advised to use low trap frequencies, such that the initial intrinsic mode can sufficiently decay.

B. Varying imbalance

Having established how the breathing modes of imbalanced droplets vary with trap frequency, this section focuses on how these modes vary with increasing imbalance. To analyze the breathing modes as a function of imbalance, the weakest trap strength studied in Fig. 2 is used, because all three imbalanced droplet breathing modes are observable.

Figure 3(a) shows an example ground-state density profile of a weakly trapped, highly imbalanced droplet with the majority and minority components shown in dark and light orange, respectively. The inset shows the density difference, $\delta n(r) = n_1(r) - n_2(r)$, between the majority and minority component. The density structure within the droplet core is comparable to the small imbalances shown in Fig. 1(a). However, the key different with a highly imbalanced mixture is the large radius gas surrounding the droplet.

Figure 3(b) highlights two examples of breathing mode oscillations for droplets with high population imbalances. The top panel shows a mixture with $\delta N_1 \approx 170267$, while the bottom panel shows a mixture with $\delta N_1 \approx 16856418$. These population imbalances are so large due to the weak trap
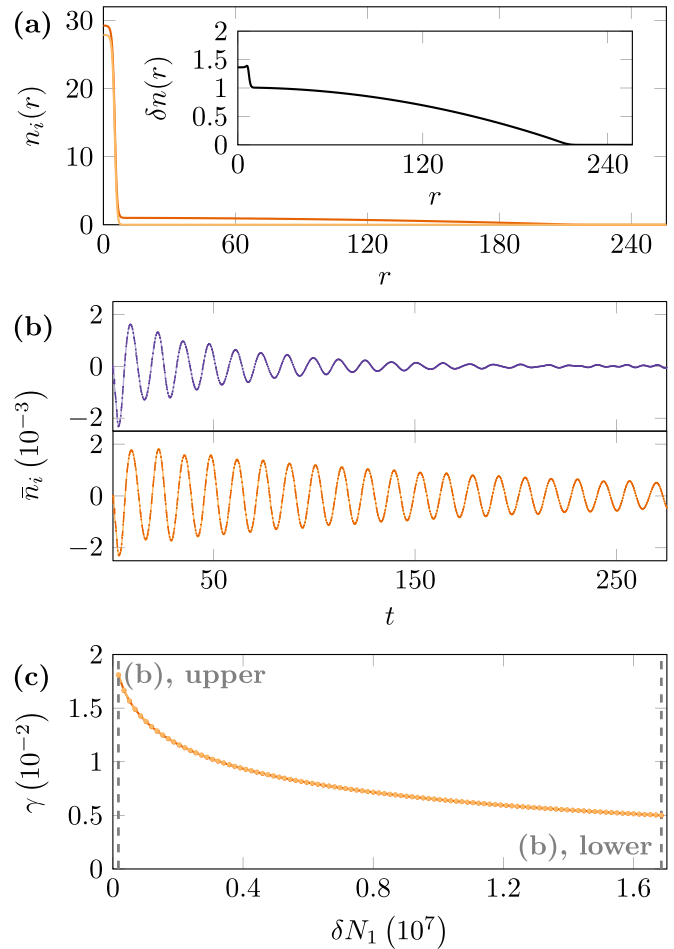

FIG. 3. Ground states and breathing modes for high imbalances in a low-frequency trap. (a) Example ground-state density profile in a trap of frequency $\omega_r \approx 0.00662$, and an imbalance of $\delta N_1 \approx 16856418$. (b) Two examples of breathing modes with a smaller imbalance of $\delta N_1 \approx 170267$ in the top panel, and a considerably larger imbalance of $\delta N_1 \approx 16856418$ in the bottom panel. These example imbalances are highlighted in (c) by the vertical dashed lines. (c) Fitted decay rate to the initial droplet breathing mode, with varying size of imbalance.

geometry used, i.e., to achieve significant gas densities in these low-frequency traps, substantial imbalances are needed. The same measure of central density as used in Fig. 2 is shown, prior to the first recombination event.

In both panels of Fig. 3(b) there does not appear to be any out-of-phase oscillations between the two components from the majority-component chemical potential mode, as shown in Fig. 2(b). The surrounding gas therefore seems to have frozen out this long-wavelength mode, similar to the higher-frequency trap in Fig. 2(c). The main difference between the top and bottom panels of Fig. 3(b) is the lower decay rate of the initial, high-amplitude mode in the more imbalanced mixture. As shown in Fig. 2(b), at later times the initial mode in the top panel has decayed sufficiently such that the minority-component chemical potential mode is visible. By driving the imbalance even higher the decay rate of the initial rate is greatly reduced, such that minority-component chemical mode cannot be observed.

In Fig. 3(c), the droplet central density is fitted to a decaying sinusoidal curve, of the form $\bar{n}_i = A e^{-\gamma t} \sin(\omega t + \phi) + c$.[2] With increasing imbalance there is a corresponding decrease in the fitted decay rate, γ. This implies that a higher surrounding gas density resists the particle emission from the droplet. This could be of potential benefit to experiments as it implies that larger imbalances would give more time to observe the decaying breathing mode oscillations.

Beyond the observation of trapped imbalanced droplets, there are also questions to be asked of the experimental realisability of a free-space imbalanced droplet. For example, how stable is the imbalance under the transition from the trap, used to prepare the mixture, to the free-space droplet.

V. RELEASE INTO FREE SPACE

This section studies the dynamics of trapped, imbalanced droplets when released into free space. This is similar to a time-of-flight (TOF) expansion, a method used in experiments in which trap potentials are switched off and the atomic cloud expands, often used for imaging. Imbalanced droplets are less stably bound than balanced droplets [45], thus the motivating question is whether it is possible to preserve the imbalance when released from a trap. This is a crucial question in the feasibility of experimentally creating a free-space, imbalanced droplet.

TOF expansion has been a widely used technique in quantum gas experiments [60] from the very first experimental observation of Bose-Einstein condensation [61,62]. Typically, by removing the trap the resulting expansion increases the scale of defects, such as vortices, accounting for the low resolution of imaging apparatus [63–65]. Measurements of condensate density from TOF images can also be used to compute approximate temperatures and population numbers of the cloud [66,67].

While most quantum gas experiments are inherently in the gas phase, droplets are by definition self-bound, liquid states [7], and hence must retain an approximately fixed size when released into free space. This property is useful for experiments as evidence for the production of quantum droplets [37–41,68], though relatively high-resolution imaging is necessary.

The two observables used here to measure the dynamics resulting from the release into free space, are the population numbers contained within the droplet, and the central droplet density difference, $\delta n(r=0) = n_1(r=0) - n_2(r=0)$. The population numbers are used to measure the particle loss from each component, while the central density difference is used as a measure of how the droplet core evolves after being released from the trap. The population numbers of the droplet are computed by

$$N_i^{\mathrm{drop}}(t) = 4\pi \int_0^{R^{\mathrm{drop}}(t)} r^2 |\Psi_i(r,t)|^2 \, dr,$$

in which $R^{\mathrm{drop}}(t)$ is defined as the radius at which the component density equals 0.1% of the maximum component density,

---

[2]Curve fitting is implemented by the optimize.curve_fit function [58] from the SciPy library for Python [59].

i.e., giving an approximate droplet radius. The population numbers are extracted in time, and $R^{\mathrm{drop}}(t)$ is allowed to vary dynamically.

A. Instantaneous trap release

To simulate the release into free space, ground states are computed as in Sec. III. The traps are then instantaneously turned off and the mixture is evolved in real time. The instant trap turn off can be quite a violent excitation of the droplet particularly with higher trap frequencies.

Figure 4(a) shows the population numbers of each component for two different initial trap frequencies: a lower frequency of $\omega_r \approx 0.0132$, given by the orange curves, and a higher frequency of $\omega_r \approx 0.261$, given by the purple curves. The droplet size is the same as in Secs. III and IV, and is within the bound, imbalanced regime ($\delta N_1 \approx 596$), i.e., there is no surrounding gas. The population numbers of both the minority (light orange) and majority (dark orange) components in the lower frequency trap remain relatively constant, as does the central density difference given in the left inset. Due to the arbitrary cutoff used, there are some small oscillations in the population numbers. In the higher-frequency trap, both the majority (light purple) and minority (dark purple) components exhibit heavy initial losses before equilibrating to a population balance. Further evidence of this density balancing is given by the zero central density difference given in the right inset.

Figure 4(a) indicates that the equilibrated population numbers following the release into free space depend on the initial trap frequency. Figure 4(b) shows the trap frequency dependency of the late-time equilibrated population numbers, $N_{i,f}$. Presented are the majority (dark orange) and minority components (light orange) of a bound, imbalanced droplet (top panel) and a saturated, imbalanced droplet surrounded by an unbound gas (bottom panel), with the equilibrated central density difference, $\delta n(r=0)_f$, inset.

The top panel of Fig. 4(b) shows that the imbalance can be approximately conserved following the release from an initial low-frequency trap, though the imbalance is lost at higher trap frequencies as demonstrated by the zero central density difference inset. Increasing the trap frequency further results in losses from both components. A larger imbalance of $\delta N_1 \approx 4257$ is given in the bottom panel, showing that the transition to balanced droplets is suppressed to higher trap frequencies. For example the central density difference drops to zero for $\omega_r \approx 0.125$ in the top panel but is shifted to $\omega_r \approx 0.2$ in the bottom panel.

B. Ramping down the trap

Having shown a population imbalance is lost when droplets are released instantaneously from a high-frequency trap, it is natural to investigate whether the imbalance can be retained when slowly released from a high-frequency trap. To do this the trap frequency is ramped down to zero in real time over a set time, t_{ramp}.

Figure 5(a) shows the population numbers in time of a droplet in a ramped-down trap of initial frequency $\omega_r \approx 0.261$. The trap frequency is ramped down by the relationship,
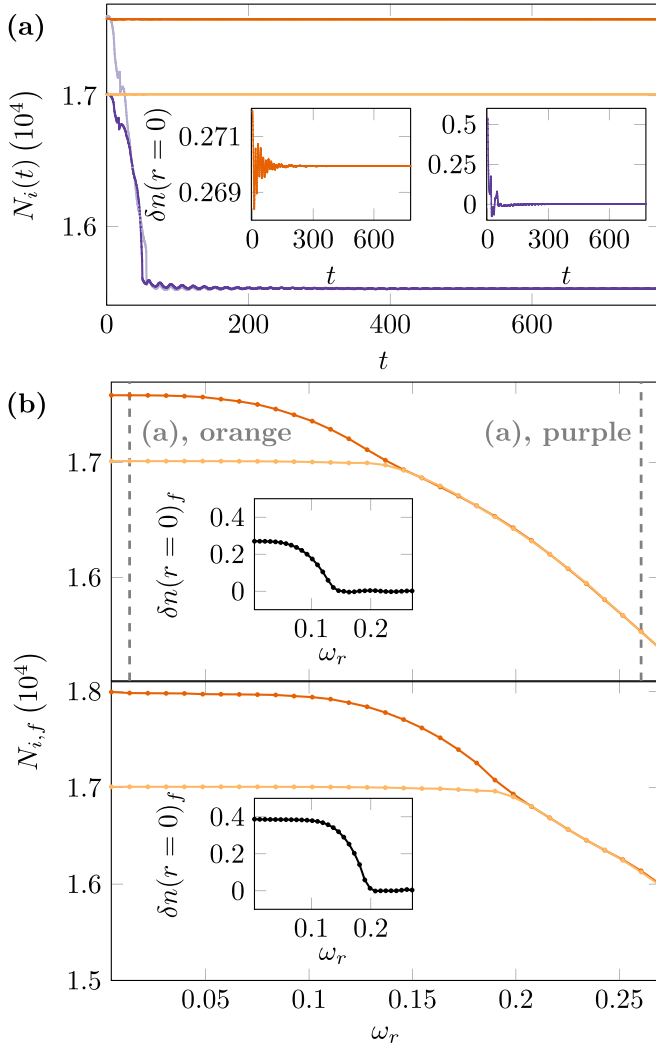
FIG. 4. Dynamics of imbalanced droplets due to an instantaneous release into free space, with the same parameters as in Figs. 1–3. (a) Population numbers varying in time following the release into free space at $t = 0$. The bound, imbalanced droplet has an initial imbalance of $\delta N_1 \approx 596$. The orange curves correspond to an initial low-frequency trap with $\omega_r \approx 0.0132$ (dark and light orange corresponding to majority and minority components, respectively), while the purple curves correspond to an initial high-frequency trap, with $\omega_r \approx 0.261$ (light and dark purple corresponding to majority and minority components, respectively). The insets show the central density differences in time, with the left and right panels corresponding to the low- and high-frequency traps, respectively. These two example simulations are highlighted in the top panel of (b) by the vertical, dashed lines. (b) The equilibrated population numbers and central density differences (inset) for varying initial trap frequencies, in the range $0.00442 \lesssim \omega_r \lesssim 0.269$. The top panel corresponds to a bound, imbalanced droplet ($\delta N_1 \approx 596$) while the bottom panel corresponds to a saturated, imbalanced droplet with an external unbound gas ($\delta N_1 \approx 4257$).

$V_i = \left(1 - t/t_{\mathrm{ramp}}\right) V_i^{\mathrm{init}}$, in which V_i^{init} is the initial trap profile. To compute the population numbers, the same method and radial cutoff as in Fig. 4 is used. The dark and light orange curves correspond to the majority and minority components, respectively, under a ramp-down time of $t_{\mathrm{ramp}} \approx 0.781$, which
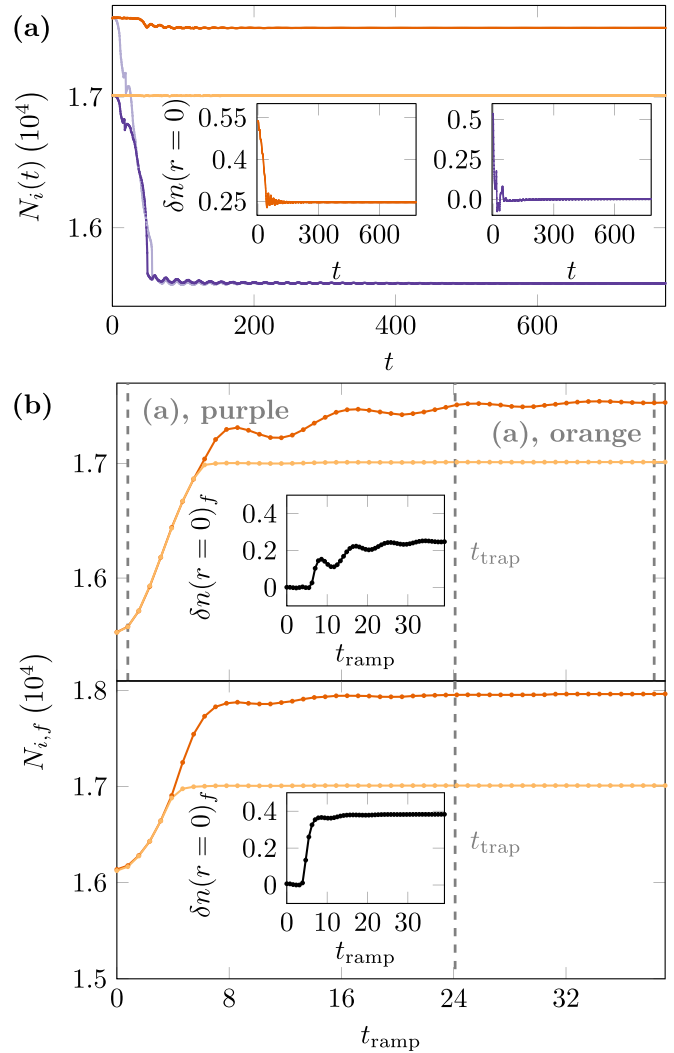
FIG. 5. Dynamics of imbalanced droplets due to a ramped down trap potential, with the same parameters as in Figs. 1–4. (a) Population numbers varying in time with the orange curves correspond to a relatively slow ramp down of $t_{\mathrm{ramp}} \approx 38.3$ (dark and light orange corresponding to majority and minority components, respectively), and purple colors corresponding to a relatively fast ramp down of $t_{\mathrm{ramp}} \approx 0.781$ (light and dark purple corresponding to majority and minority components, respectively). The insets show the central density differences in time, with the left and right panels corresponding to the slow and fast ramps, respectively. These two example simulations are highlighted in the top panel of (b), by the vertical, dashed lines. (b) The equilibrated population numbers and central density differences (inset) for varying ramp-down times, t_{ramp}, in the range $0.0 \leqslant t_{\mathrm{ramp}} \lesssim 39.1$. The top panel corresponds to a bound, imbalanced droplet ($\delta N_1 \approx 596$) while the bottom panel corresponds to a saturated, imbalanced droplet with an external unbound gas ($\delta N_1 \approx 4257$).

is fast relative to the trap period, $t_{\mathrm{trap}} \approx 24.1$. Both components undergo heavy losses before equilibrating to balanced population numbers, and zero central density difference, comparable to the high-frequency instantaneous trap release given by the purple curves in Fig. 4(a). The dark and light purple curves correspond to the minority and majority components, respectively, under a ramp-down time of $t_{\mathrm{ramp}} \approx 38.3$, which

is slow relative to the trap period, t_{trap}. There are some small losses primarily from the majority component; however, the imbalance is largely retained during these ramp-down dynamics. Furthermore, the central density difference of a trapped droplet is larger than that of a free-space imbalanced droplet as highlighted in Figs. 1(a) and 1(b). The left inset of Fig. 5(a) shows that the central density difference initially decreases but stabilizes at a nonzero value. Thus, the imbalance can be retained under the release from a high-frequency trap, though the trap must be ramped down sufficiently slowly.

Figure 5(b) shows the ramp-down time, t_{ramp}, dependency of the final equilibrated population numbers and central density difference (inset). The top panel considers a bound, imbalanced droplet showing that fast ramps result in balanced droplets that undergo losses from both components though slower ramps can retain some atoms in both components. Increasing the ramp-down time above $t_{ramp} \approx 8$ indicates that the original imbalance can be approximately retained. A saturated, imbalanced droplet with an unbound cloud is given in the bottom panel of Fig. 5(b) and likewise shows that fast ramps result in balanced droplets, while slower ramps yield a preservation of some imbalance. Note that the initial imbalance is not retained in the bottom panel, because the unbound cloud will always be lost in free space, i.e., the resulting droplet is approximately a saturated, imbalanced droplet in free space.

To summarize, an imbalanced droplet prepared in a relatively low-frequency trap can retain the majority of the initial imbalance after an instantaneous release into free space. With increasing trap frequency, the majority component will lose atoms until no imbalance is retained. The loss of imbalance can, in general, be suppressed by increasing the initial imbalance, lowering the initial trap frequency, or lengthening the ramp-down time. These results show that imbalanced droplets can be robust to a release into free space suggesting that free-space, imbalanced droplets are feasible using modern experimental techniques.

VI. DISCUSSION

This work has investigated ground states, breathing modes and the release into free space of imbalanced droplets confined in isotropic harmonic traps. First, Sec. III demonstrates that the trapping potential squeezes any unbound gas up to the droplet, forming a significant gas density at the droplet surface. The imbalance-dependent divergence in the majority- and minority-component chemical potentials, increases further with higher trap frequencies.

Section IV focuses on the breathing modes of imbalanced droplets, and contrasts the trapped geometry with the free-space results of Ref. [45]. This section highlights that the presence of a trap causes recombination events from reflected particles. For a free-space imbalanced droplet there are three breathing mode frequencies [45]. These three modes can be observed in the trapped, imbalanced droplet though Sec. IV shows that with increasing trap frequency these modes are

lost. Similarly the decay rate of the imbalanced droplet breathing mode can be reduced by the presence of a significant majority-component gas.

The final results presented are the dynamics of releasing imbalanced droplets into free space given in Sec. V. The results show primarily that with a low-frequency initial trap, the droplet imbalance can be preserved under an instantaneous release, though higher trap frequencies lead to a loss of the imbalance. However, a droplet released from a higher-frequency trap can preserve its imbalance by ramping down the trap. This gives promise for the experimental realization of free-space, imbalanced quantum droplets.

The stability of the imbalance under release from a trap may be significant in the experimental results of Refs. [36,38], in which the mixture is prepared with $N_2/N_1 = 1 \neq \sqrt{a_{11}/a_{22}}$. These works assume that the droplet will dynamically balance, after the release into free space, to $N_2/N_1 = \sqrt{a_{11}/a_{22}}$. This could explain why the data points of N_1/N_2 in Fig. 4(c) of Ref. [38] are upshifted from the balanced line of $N_2/N_1 = \sqrt{a_{11}/a_{22}}$, as component 1 is set up to be the majority component. Likewise, some of the results in Ref. [39] are speculated to be sensitive to imbalance. This work suggests that balanced droplets could be a special case, and that imbalanced droplets are more common.

The analysis of spherically symmetric ground states and breathing mode dynamics presented could be extended to explore heteronuclear mixtures. The different kinetic energy contributions of the two components may lead to novel physics, as adding an imbalance to either component is no longer symmetric. This is, however, a nontrivial extension due to the form of the two-component LHY correction of a heteronuclear mixture [7,33].

The recombination events from the trap limit the time for observing collective modes. This restriction implies that smaller computational boxes could be used to probe collective modes in more general 3D simulations, allowing for observation of nonzero angular momentum modes such as dipole [53,68] and quadrupole modes in both balanced and imbalanced droplets.

The potential of new mixtures for probing droplet physics is exciting but some experiments use highly anisotropic trap potentials with significant population number imbalances [69]. Therefore it is vital to understand how droplets are modified from the prototypical balanced, free-space profile, by population imbalances and trap potentials.

The data presented in this paper are available [70].

[1] I. Bloch, Ultracold quantum gases in optical lattices, Nature Phys. **1**, 23 (2005).

[2] I. Bloch, J. Dalibard, and W. Zwerger, Many-body physics with ultracold gases, Rev. Mod. Phys. **80**, 885 (2008).

[3] I. Bloch, J. Dalibard, and S. Nascimbène, Quantum simulations with ultracold quantum gases, Nat. Phys. **8**, 267 (2012).

[4] T. Roger, C. Maitland, K. Wilson, N. Westerberg, D. Vocke, E. M. Wright, and D. Faccio, Optical analogues of the Newton–Schrödinger equation and boson star evolution, Nat. Commun. **7**, 13492 (2016).

[5] S. Eckel, A. Kumar, T. Jacobson, I. B. Spielman, and G. K. Campbell, A rapidly expanding Bose-Einstein condensate: An expanding universe in the lab, Phys. Rev. X **8**, 021021 (2018).

[6] N. Proukakis, D. Snoke, and P. Littlewood, *Universal Themes of Bose-Einstein Condensation* (Cambridge University Press, Cambridge, 2017).

[7] D. S. Petrov, Quantum mechanical stabilization of a collapsing Bose-Bose mixture, Phys. Rev. Lett. **115**, 155302 (2015).

[8] D. S. Petrov, Liquid beyond the Van der Waals paradigm, Nat. Phys. **14**, 211 (2018).

[9] P. Courteille, R. S. Freeland, D. J. Heinzen, F. A. van Abeelen, and B. J. Verhaar, Observation of a Feshbach resonance in cold atom scattering, Phys. Rev. Lett. **81**, 69 (1998).

[10] S. Inouye, M. R. Andrews, J. Stenger, H.-J. Miesner, D. M. Stamper-Kurn, and W. Ketterle, Observation of Feshbach resonances in a Bose-Einstein condensate, Nature (London) **392**, 151 (1998).

[11] C. Chin, R. Grimm, P. Julienne, and E. Tiesinga, Feshbach resonances in ultracold gases, Rev. Mod. Phys. **82**, 1225 (2010).

[12] T. D. Lee, K. Huang, and C. N. Yang, Eigenvalues and eigenfunctions of a Bose system of hard spheres and its low-temperature properties, Phys. Rev. **106**, 1135 (1957).

[13] J. L. Roberts, N. R. Claussen, S. L. Cornish, E. A. Donley, E. A. Cornell, and C. E. Wieman, Controlled collapse of a Bose-Einstein condensate, Phys. Rev. Lett. **86**, 4211 (2001).

[14] E. A. Donley, N. R. Claussen, S. L. Cornish, J. L. Roberts, E. A. Cornell, and C. E. Wieman, Dynamics of collapsing and exploding Bose-Einstein condensates, Nature (London) **412**, 295 (2001).

[15] F. Böttcher, J.-N. Schmidt, J. Hertkorn, K. S. H. Ng, S. D. Graham, M. Guo, T. Langen, and T. Pfau, New states of matter with fine-tuned interactions: Quantum droplets and dipolar supersolids, Rep. Prog. Phys. **84**, 012403 (2021).

[16] Z.-H. Luo, W. Pang, B. Liu, Y.-Y. Li, and B. A. Malomed, A new form of liquid matter: Quantum droplets, Front. Phys. **16**, 32201 (2021).

[17] D. S. Petrov and G. E. Astrakharchik, Ultradilute low-dimensional liquids, Phys. Rev. Lett. **117**, 100401 (2016).

[18] T. Ilg, J. Kumlin, L. Santos, D. S. Petrov, and H. P. Büchler, Dimensional crossover for the beyond-mean-field correction in Bose gases, Phys. Rev. A **98**, 051604(R) (2018).

[19] P. Zin, M. Pylak, T. Wasak, M. Gajda, and Z. Idziaszek, Quantum Bose-Bose droplets at a dimensional crossover, Phys. Rev. A **98**, 051603(R) (2018).

[20] H. Kadau, M. Schmitt, M. Wenzel, C. Wink, T. Maier, I. Ferrier-Barbut, and T. Pfau, Observing the Rosensweig instability of a quantum ferrofluid, Nature (London) **530**, 194 (2016).

[21] I. Ferrier-Barbut, H. Kadau, M. Schmitt, M. Wenzel, and T. Pfau, Observation of quantum droplets in a strongly dipolar Bose gas, Phys. Rev. Lett. **116**, 215301 (2016).

[22] M. Schmitt, M. Wenzel, F. Böttcher, I. Ferrier-Barbut, and T. Pfau, Self-bound droplets of a dilute magnetic quantum liquid, Nature (London) **539**, 259 (2016).

[23] L. Chomaz, S. Baier, D. Petter, M. J. Mark, F. Wächtler, L. Santos, and F. Ferlaino, Quantum-fluctuation-driven crossover from a dilute Bose-Einstein condensate to a macrodroplet in a dipolar quantum fluid, Phys. Rev. X **6**, 041039 (2016).

[24] T. Lahaye, C. Menotti, L. Santos, M. Lewenstein, and T. Pfau, The physics of dipolar bosonic quantum gases, Rep. Prog. Phys. **72**, 126401 (2009).

[25] F. Wächtler and L. Santos, Quantum filaments in dipolar Bose-Einstein condensates, Phys. Rev. A **93**, 061603(R) (2016).

[26] R. N. Bisset, R. M. Wilson, D. Baillie, and P. B. Blakie, Ground-state phase diagram of a dipolar condensate with quantum fluctuations, Phys. Rev. A **94**, 033619 (2016).

[27] S. Pal, D. Baillie, and P. B. Blakie, Excitations and number fluctuations in an elongated dipolar Bose-Einstein condensate, Phys. Rev. A **102**, 043306 (2020).

[28] A.-C. Lee, D. Baillie, and P. B. Blakie, Numerical calculation of dipolar-quantum-droplet stationary states, Phys. Rev. Res. **3**, 013283 (2021).

[29] S. Pal, D. Baillie, and P. B. Blakie, Infinite dipolar droplet: A simple theory for the macrodroplet regime, Phys. Rev. A **105**, 023308 (2022).

[30] C. F. Barenghi, R. J. Donnelly, and W. Vinen, *Quantized Vortex Dynamics and Superfluid Turbulence*, Vol. 571 (Springer Science & Business Media, Berlin, 2001).

[31] C. F. Barenghi, L. Skrbek, and K. R. Sreenivasan, Introduction to quantum turbulence, Proc. Natl. Acad. Sci. USA **111**, 4647 (2014).

[32] C. F. Barenghi, H. A. J. Middleton-Spencer, L. Galantucci, and N. G. Parker, Types of quantum turbulence, AVS Quantum Science **5**, 025601 (2023).

[33] F. Ancilotto, M. Barranco, M. Guilleumas, and M. Pi, Self-bound ultradilute Bose mixtures within local density approximation, Phys. Rev. A **98**, 053623 (2018).

[34] V. Cikojević, E. Poli, F. Ancilotto, L. Vranješ-Markić, and J. Boronat, Dilute quantum liquid in a K-Rb Bose mixture, Phys. Rev. A **104**, 033319 (2021).

[35] D. Baillie, R. M. Wilson, and P. B. Blakie, Collective excitations of self-bound droplets of a dipolar quantum fluid, Phys. Rev. Lett. **119**, 255302 (2017).

[36] G. Ferioli, G. Semeghini, L. Masi, G. Giusti, G. Modugno, M. Inguscio, A. Gallemí, A. Recati, and M. Fattori, Collisions of self-bound quantum droplets, Phys. Rev. Lett. **122**, 090401 (2019).

[37] C. R. Cabrera, L. Tanzi, J. Sanz, B. Naylor, P. Thomas, P. Cheiney, and L. Tarruell, Quantum liquid droplets in a mixture of Bose-Einstein condensates, Science **359**, 301 (2018).

[38] G. Semeghini, G. Ferioli, L. Masi, C. Mazzinghi, L. Wolswijk, F. Minardi, M. Modugno, G. Modugno, M. Inguscio, and M. Fattori, Self-bound quantum droplets of atomic mixtures in free space, Phys. Rev. Lett. **120**, 235301 (2018).

[39] P. Cheiney, C. R. Cabrera, J. Sanz, B. Naylor, L. Tanzi, and L. Tarruell, Bright soliton to quantum droplet transition in a mixture of Bose-Einstein condensates, Phys. Rev. Lett. **120**, 135301 (2018).

[40] C. D'Errico, A. Burchianti, M. Prevedelli, L. Salasnich, F. Ancilotto, M. Modugno, M. Minardi, and C. Fort, Observation of quantum droplets in a heteronuclear bosonic mixture, Phys. Rev. Res. **1**, 033155 (2019).

[41] Z. Guo, F. Jia, L. Li, Y. Ma, J. M. Hutson, X. Cui, and D. Wang, Lee-Huang-Yang effects in the ultracold mixture of ^{23}Na and

^{87}Rb with attractive interspecies interactions, Phys. Rev. Res. **3**, 033247 (2021).

[42] T. Mithun, A. Maluckov, K. Kasamatsu, B. A. Malomed, and A. Khare, Modulational instability, inter-component asymmetry, and formation of quantum droplets in one-dimensional binary Bose gases, Symmetry **12**, 174 (2020).

[43] M. N. Tengstrand and S. M. Reimann, Droplet-superfluid compounds in binary bosonic mixtures, Phys. Rev. A **105**, 033319 (2022).

[44] J. Vallès-Muns, I. Morera, G. E. Astrakharchik, and B. Juliá-Díaz, Quantum droplets with particle imbalance in one-dimensional optical lattices, arXiv:2306.12283.

[45] T. A. Flynn, L. Parisi, T. P. Billam, and N. G. Parker, Quantum droplets in imbalanced atomic mixtures, Phys. Rev. Res. **5**, 033167 (2023).

[46] F. Ancilotto, M. Barranco, and M. Pi, Breakup of quantum liquid filaments into droplets, Phys. Rev. A **107**, 063312 (2023).

[47] J. C. Smith, D. Baillie, and P. B. Blakie, Quantum droplet states of a binary magnetic gas, Phys. Rev. Lett. **126**, 025302 (2021).

[48] R. N. Bisset, L. A. Peña Ardila, and L. Santos, Quantum droplets of dipolar mixtures, Phys. Rev. Lett. **126**, 025301 (2021).

[49] T.-L. Ho and V. B. Shenoy, Binary mixtures of Bose condensates of alkali atoms, Phys. Rev. Lett. **77**, 3276 (1996).

[50] Q. Gu and L. Yin, Phonon stability and sound velocity of quantum droplets in a boson mixture, Phys. Rev. B **102**, 220503(R) (2020).

[51] Y. Xiong and L. Yin, Effective single-mode model of a binary boson mixture in the quantum droplet region, Phys. Rev. A **105**, 053305 (2022).

[52] T. Bienaimé, E. Fava, G. Colzi, C. Mordini, S. Serafini, C. Qu, S. Stringari, G. Lamporesi, and G. Ferrari, Spin-dipole oscillation and polarizability of a binary Bose-Einstein condensate near the miscible-immiscible phase transition, Phys. Rev. A **94**, 063652 (2016).

[53] A. Cappellaro, T. Macrì, and L. Salasnich, Collective modes across the soliton-droplet crossover in binary Bose mixtures, Phys. Rev. A **97**, 053623 (2018).

[54] H. Hu and X.-J. Liu, Collective excitations of a spherical ultradilute quantum droplet, Phys. Rev. A **102**, 053303 (2020).

[55] L. Pitaevskii and S. Stringari, *Bose-Einstein Condensation and Superfluidity*, Vol. 164 (Oxford University Press, Oxford, 2016).

[56] S. Stringari, Collective excitations of a trapped Bose-condensed gas, Phys. Rev. Lett. **77**, 2360 (1996).

[57] C. Fort and M. Modugno, Self-evaporation dynamics of quantum droplets in a ^{41}K-^{87}Rb mixture, Appl. Sci. **11**, 866 (2021).

[58] K. W. Vugrin, L. P. Swiler, R. M. Roberts, N. J. Stucky-Mack, and S. P. Sullivan, Confidence region estimation techniques for nonlinear regression in groundwater flow: Three case studies, Water Resour. Res. **43**, 004804 (2007).

[59] P. Virtanen, R. Gommers, T. E. Oliphant, M. Haberland, T. Reddy, D. Cournapeau, E. Burovski, P. Peterson, W. Weckesser, J. Bright, S. J. van der Walt, M. Brett, J. Wilson, K. J. Millman, N. Mayorov, A. R. J. Nelson, E. Jones, R. Kern, E. Larson, C. J. Carey *et al.*, SciPy 1.0: Fundamental algorithms for scientific computing in Python, Nat. Meth. **17**, 261 (2020).

[60] Y. Castin and R. Dum, Bose-Einstein condensates in time dependent traps, Phys. Rev. Lett. **77**, 5315 (1996).

[61] M. H. Anderson, J. R. Ensher, M. R. Matthews, C. E. Wieman, and E. A. Cornell, Observation of Bose-Einstein condensation in a dilute atomic vapor, Science **269**, 198 (1995).

[62] K. B. Davis, M.-O. Mewes, M. R. Andrews, N. J. van Druten, D. S. Durfee, D. M. Kurn, and W. Ketterle, Bose-Einstein condensation in a gas of sodium atoms, Phys. Rev. Lett. **75**, 3969 (1995).

[63] K. W. Madison, F. Chevy, W. Wohlleben, and J. Dalibard, Vortex formation in a stirred Bose-Einstein condensate, Phys. Rev. Lett. **84**, 806 (2000).

[64] C. Raman, J. R. Abo-Shaeer, J. M. Vogels, K. Xu, and W. Ketterle, Vortex nucleation in a stirred Bose-Einstein condensate, Phys. Rev. Lett. **87**, 210402 (2001).

[65] J. R. Abo-Shaeer, C. Raman, J. M. Vogels, and W. Ketterle, Observation of vortex lattices in Bose-Einstein condensates, Science **292**, 476 (2001).

[66] J. R. Ensher, D. S. Jin, M. R. Matthews, C. E. Wieman, and E. A. Cornell, Bose-Einstein condensation in a dilute gas: Measurement of energy and ground-state occupation, Phys. Rev. Lett. **77**, 4984 (1996).

[67] D. M. Stamper-Kurn, H.-J. Miesner, A. P. Chikkatur, S. Inouye, J. Stenger, and W. Ketterle, Reversible formation of a Bose-Einstein condensate, Phys. Rev. Lett. **81**, 2194 (1998).

[68] L. Cavicchioli, C. Fort, M. Modugno, F. Minardi, and A. Burchianti, Dipole dynamics of an interacting bosonic mixture, Phys. Rev. Res. **4**, 043068 (2022).

[69] K. E. Wilson, A. Guttridge, J. Segal, and S. L. Cornish, Quantum degenerate mixtures of Cs and Yb, Phys. Rev. A **103**, 033306 (2021).

[70] Doi: 10.25405/data.ncl.24085248.